analytical chemistry

pubs.acs.org/ac Article

Absorbance Detection in Multireflection Microfluidic Channels Using a Commercial Microplate Reader System

Naoki Yanagisawa, Sakur Mahmud, and Debashis Dutta*

Cite This: *Anal. Chem.* 2020, 92, 13050–13057 Read Online

ACCESS | Metrics & More | Article Recommendations

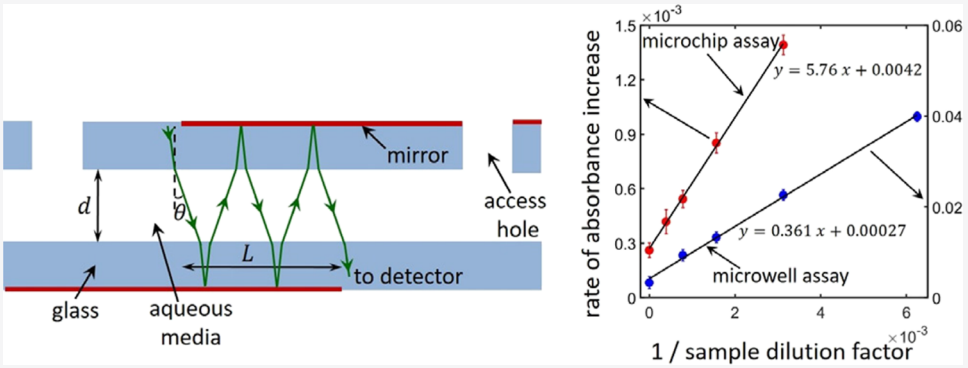

ABSTRACT: Absorbance detection is often prohibited in microfluidic channels due to the limited optical path length available in these systems. However, this optical distance may be significantly increased by guiding the probing light beam along the channel length via multiple reflections by patterned metallic surfaces. In this work, we demonstrate enhanced absorbance detection in glass microfluidic channels using a commercial microplate reader based on this principle, yielding detection limits comparable to that measured on standard microwell plates. This improvement in detectability was realized through careful optimization of the mirror lengths and locations combined with the appropriate design of a microchip holder to suitably position the microchannels in the microplate reader. Additionally, it was determined that the angle by which our device was tilted relative to the horizontal plane played an important role in this optimization. For an optimum choice of parameters accessible with our design, the sensitivity of our absorbance measurements in a 30 μm-deep channel was improved by as much as 52-fold, raising this quantity to about 84% of the corresponding value realized for 75 μL samples placed within 7 mm i.d. standard cylindrical microwells. Quantitative ELISAs employing the absorbance detection method were demonstrated on the noted multireflection microchip device for assessing West Nile viral IgM antibody levels in human serum samples yielding analyte detection limits comparable to that measured on standard microwell plates.

Miniaturization of liquid-phase assays often allows significant improvements in performance metrics as well as substantial time and cost savings.[1−4] As a result, there has been a concerted effort by the scientific community toward developing formats that allow assay implementation at shorter length scales. In this regard, the emergence of micro- and nanofluidic systems over the past three decades has shown significant promise for assay miniaturization and automation.[5−9] Moreover, the greater control over analyte transport realizable in these systems has permitted efficient integration of multiple analytical procedures on a single footprint, leading to the development of several standalone "lab-on-a-Chip" platforms.[10,11] However, perhaps, most interestingly, such miniaturization has allowed the development of novel assays with advanced analytical capabilities exploiting some of the physical phenomena uniquely prominent at the micro- and nanometer length scales.[12,13] However, a significant disadvantage to reducing the size of the assay chamber is often a decreased detection sensitivity for the analyte molecules.[14] For example, absorbance detection methods are often prohibited in microfluidic channels due to the limited optical path length available in these systems. In addition, micro-/nanofluidic devices tend to be frequently incompatible with commercial instruments, such as microplate readers, making their adoption difficult by scientists with limited background on instrumentation.

Received: May 6, 2020
Accepted: August 28, 2020
Published: August 28, 2020

https://dx.doi.org/10.1021/acs.analchem.0c01961
Anal. Chem. 2020, 92, 13050−13057

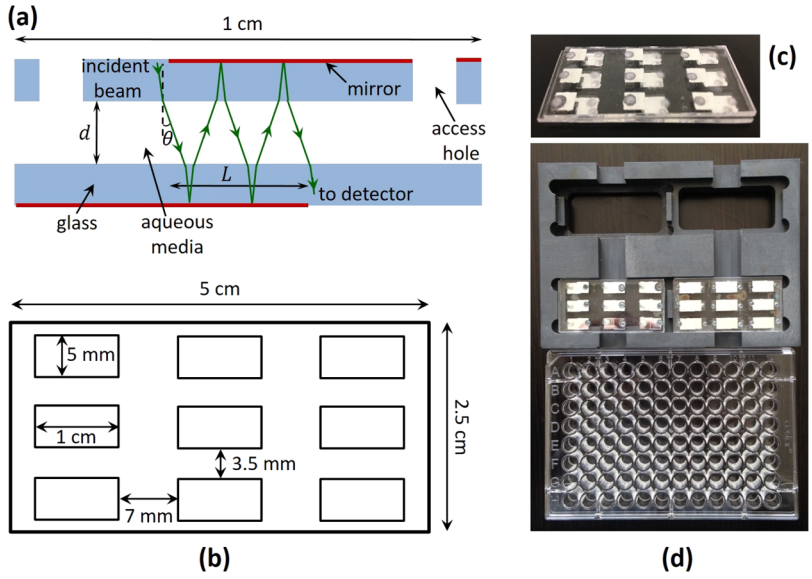

Figure 1. (a) Schematic of the multireflection process occurring in our glass microchannels. (b) Layout photolithographically patterned on our microchip devices to fabricate 5 mm-wide fluidic channels/mirrors. (c) Image of a microchip used in this work. (d) Image of the microchip holder made out of polyvinyl chloride (PVC) employed in the current work. The external dimensions of the noted PVC holder were matched to that of a commercial microwell plate, that is, 12.7 × 8.5 cm, in order to render it compatible with a commercial microplate reader system. Note that the exact location of the access holes varied marginally for the different microchannels on our microchip as they were punched using a microabrasive powder blasting system after manually determining the edge of the channels.

Two major strategies have been commonly adopted to improve the detection sensitivity of microfluidic devices. They include the integration of preconcentration techniques and incorporation of advanced detection systems that help increase the signal-to-noise ratio for a chosen measurement. Microchip-based preconcentration techniques that allow trapping of molecular species and/or larger entities, such as biological cells and particulate matter, within a detection region have been extensively reported in the literature. A wide range of forces, including electric,[15] magnetic,[16] acoustic,[17] and hydrodynamic[18] fields, have been employed to realize this capability with an impressive level of success. In addition, preconcentration approaches involving the capture of analyte molecules onto a target surface[19] or their extraction into a desired solvent[20] have been also explored, although their integration to various microchip operations tends to be more challenging particularly in comparison with the electric field-based sample-stacking techniques. The incorporation of advanced detection systems into microchip platforms including those relying on optical-based,[14] electrochemical-based,[21] electrical conductivity-based,[22] and mass spectrometry-based[23] sensing methods has been explored as another important avenue for improving the detection sensitivity of micro-/nanofluidic devices. Among these developments, the integration of advanced optical sensing modules has been pursued to a large extent likely due to their utility in quantitating a wide range of samples as well as extremely small analyte concentrations.

Advancements made on integrating absorbance-based detection methods to microchip devices, however, have not received much attention from the research community over the years.[14] As such, in spite of its applicability to a wide range of analytes, this sensing technique has proven unattractive for miniaturized platforms due to the need for relatively long optical path lengths. Moreover, the effort needed to enable absorbance detection in microfluidic systems tends to be significant as well, deterring its use by researchers with limited background on instrumentation. To address these issues, we demonstrate absorbance detection in multireflection microfluidic channels using a commercial microplate reader yielding analyte detection limits comparable to that measured on a standard microwell plate. The use of internal reflections to enhance the sensitivity of optical detection methods in microfluidic systems has been previously explored in the literature for a variety of applications. For example, such reflections have been employed in designing refractometers for sensitive temperature and strain measurements.[24,25] In a different work, ATR-FTIR internal reflection elements were incorporated in microfluidic devices for chemical imaging applications.[26] The use of air pockets to allow multireflection of optical light has been also demonstrated, allowing significant improvements in absorbance- and fluorescence-based sensing in microchannels.[27] Furthermore, enhanced absorbance measurements were realized for microchip-based capillary electrophoretic assays using patterned metal surfaces by Salimi-Moosavi and co-workers[28] similar to the strategy adopted in our device. Specifically, the probing light beam was guided along the channel length via multiple reflections by patterned metallic surfaces in both these works to increase the optical path length in the system. In our current work, we additionally designed a holder to suitably position the microchannels for direct quantitation of our assays using a microplate reader without having to modify this commercial instrument.[29] Optimization of the mirror lengths and tilt angles for the microchip device then allowed an improvement in the sensitivity of our absorbance measurements by as much as 52-fold in a 30 μm-deep channel, raising this quantity to about 84% of the corresponding value realized for 75 μL samples placed within 7 mm i.d. standard cylindrical microwells. Quantitative ELISAs employing the absorbance detection method were demonstrated on the noted multireflection microchip device for assessing West Nile (WN) viral IgM antibody levels in human serum samples yielding analyte

https://dx.doi.org/10.1021/acs.analchem.0c01961
Anal. Chem. 2020, 92, 13050−13057

detection limits comparable to that measured on standard microwell plates.

EXPERIMENTAL SECTION

Device Fabrication. The microfluidic devices employed in this work were fabricated using bottom and cover plates made from borosilicate glass purchased by Telic Company (Valencia, CA). These glass plates came with a thin layer of chromium and photoresist laid down on one of their surfaces to enable the photopatterning process. Photomasks custom-designed by Fineline Imaging Inc. (Colorado Springs, CO) were used to pattern the desired channel and mirror layouts using standard photolithographic methods.[30,31] To create the microchannels in our device, a layout comprising nine straight channels aligned parallel to each other (see Figure 1b) was patterned on the bottom plate with each channel being 1 cm long and 5 mm wide. After completion of the photopatterning process, the photoresist layer was cured in the microposit developer MF-319 (Rohm and Haas) and the chromium layer was removed within the patterned regions using a chromium etchant (Transene Inc.). The bottom plate was then etched to a depth between 10 and 30 μm using a buffered oxide etchant (Transene Inc.) to realize the microchannels on it. The mirror surfaces on the bottom plate were patterned by coating its clear side with a thin layer of photoresist (S1805; Rohm and Haas) using a spin-coater (Laurell Technologies) operated at 500 rpm for 10 s. A photomask very similar to that depicted in Figure 1b was used for this purpose followed by curing the glass plate with the microposit developer MF-319. While the longer edges of the mirror patterns were exactly aligned with those of the microchannels, the shorter edges were positioned variably within the channel patterns depending on the desired mirror size. To allow better adhesion of the aluminum layer within this pattern, the exposed glass surface on the bottom plate was etched with the buffered oxide etchant (BOE) to a depth of 500 nm. The mirror pattern on the cover plate was similarly realized by photolithographically transferring a suitable layout on its face with the photoresist coating. This pattern was identical to the one used for creating the mirror surfaces on the bottom plate except that was shifted along the channel axis by a fixed distance to realize the desired extent of mirror overlap denoted by the parameter L in Figure 1a. Also, in all our designs, it was ensured that the center of the mirror overlap region always coincided with that of the channel and the incident light beam in the microplate reader system to maintain symmetry. As before, following the photopatterning of the cover plate, it was sequentially cured in MF-319, the chromium etchant solution, and the BOE to etch out a 500 nm-deep region. A 300 nm layer of aluminum was then deposited over the mirror patterns on the bottom and cover plates using a metal evaporator system (Energy Beam Sciences, Inc.) to realize the reflective surfaces.[32] It must be noted however that prior to depositing the aluminum layers or etching the glass surfaces within a patterned region using BOE, the opposite face of the concerned glass plate was always manually coated with a layer of photoresist (S1805) and dried in a convection oven at 80 °C for 20 min to protect it from unwanted metal deposition and roughening/alteration by wet etching, respectively. Access holes were drilled at the channel terminals using a microabrasive powder blasting system (Vaniman Inc.) to allow the introduction of liquid reagents/samples into the microchannels. Finally, the microfluidic channels were sealed off by bringing together the bottom and cover plates in deionized water after aligning the mirror surfaces appropriately and then allowing the two plates to bond overnight in a convection oven at 80 °C.[33,34] No external reservoirs were affixed over the access holes in order to minimize the wastage of samples and assay reagents during their incubation as well as prevent any mechanical interference from these attachments while inserting our microfluidic device into the microplate reader. A holder having the dimensions of a standard microwell plate (12.7 × 8.5 × 1.5 cm) was built to accommodate our microchip devices during the signal measurement process (see Figure 1c). This holder was machined in-house out of a polyvinyl chloride (PVC) sheet and was capable of supporting up to four of our 2″ × 1″ glass microchips.[29]

Preparation of the ELISA Surface. The microchannels were activated for protein attachment by treating them with 1 M NaOH (Sigma-Aldrich) for 20 min followed by sequentially rinsing them with deionized water and methanol (Fisher Scientific) for 10 min each. These conduits were then dried at 80 °C in a forced-air convection oven for 15 min and later derivatized with (3-aminopropyl)triethoxysilane (Sigma-Aldrich) for 1 h under ambient conditions. The resulting glass surface was subsequently rinsed with methanol, dried again at 80 °C, and reacted for another 1 h with an aqueous solution of 5% w/v glutaric dialdehyde (Sigma-Aldrich) at room temperature to create a surface that could be covalently attached to the amine groups on a protein molecule.[34] The excess glutaric dialdehyde was later removed from the microchannels by washing them with deionized water to realize our "modified glass surface" as shown in Figure 2. This surface was then

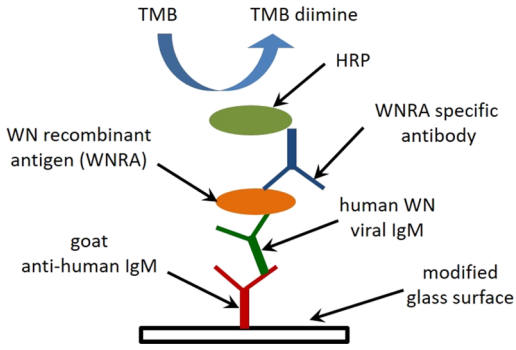

Figure 2. Schematic of the ELISA surface used for determining the levels of WN viral IgM antibody in human serum samples. The modified glass surface here refers to a glass surface sequentially derivatized with (3-aminopropyl)triethoxysilane and glutaric dialdehyde. The terms HRP and TMB in the figure refer to the enzyme label, horseradish peroxidase, and enzyme substrate, 3,3′,5,5′ tetramethylbenzidiene, respectively, used in our experiments.

prepared for a WN viral IgM assay by incubating it with a 5 μg/mL solution of goat anti-human IgM (Sigma-Aldrich) prepared in a 0.1 M sodium phosphate buffer (pH 7.4) for an hour. The unreacted sites on the surface were subsequently blocked by reacting with solutions of 1% BSA and 0.1 M lysine (both prepared in the phosphate buffer) for 20 min each.[31] A chosen dilution of the WN viral IgM antibody sample was introduced into the microchannel at this point and retained for 1 h followed by sequentially treating this assay chamber with solutions of a WN recombinant antigen (WNRA) and a WNRA-specific antibody conjugated to horseradish peroxidase (HRP) for an hour each (see Figure 2). The WN viral IgM

https://dx.doi.org/10.1021/acs.analchem.0c01961
Anal. Chem. 2020, 92, 13050−13057

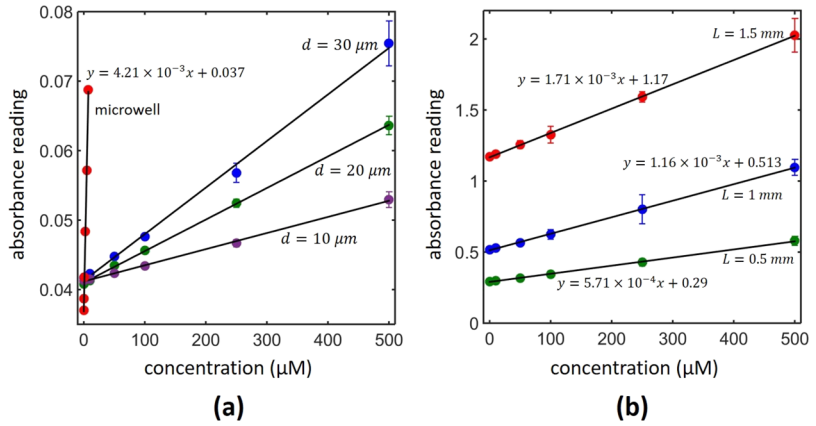

Figure 3. (a) Absorbance measurements made on BTB samples contained in standard microwells and glass microchannels (of depth d). In the figure above, the sample volume used for the microwell measurements was 75 μL and the microchannels employed were chosen to be 5 mm wide. The equations for the best-fitted lines to the data obtained from the 10, 20, and 30 μm-deep channels were $y = 2.32 \times 10^{-5}x + 0.041$, $y = 4.54 \times 10^{-5}x + 0.041$, and $y = 6.7 \times 10^{-5}x + 0.041$, respectively. (b) Effect of the extent of axial overlap of the mirror surfaces along the top and bottom glass plates, that is, parameter L in Figure 1a, on the absorbance readings made using 5 mm-wide and 30 μm-deep microchannels. The error bars in both subfigures were estimated based on five independent experiments performed in different microchannels using aliquots of the same sample.

antibody sample, WNRA, and the detection antibody−HRP conjugate used in these experiments were obtained as part of a commercial ELISA kit (catalog # WNMS-1) purchased from InBios International Inc. The microwell-based ELISAs for the WN viral IgM antibody were performed using plates purchased from InBios International Inc. that came with goat anti-human IgM−coated microwells. The microwells from this point onward were prepared for an assay following the same sequence of incubations as described for the microfluidic ELISAs. However, while the microchip-based experiments required only 3 μL of the assay reagents, this quantity for the microwell ELISAs was 75 μL. All reagents and samples were loaded into the microchips and microwells using commercial micropipettes. To minimize contamination of the various ELISA components in the analysis chamber, all incubations in the microchannels and microwells were separated by 20 and 200 μL buffer washes, respectively. The solutions used for this purpose were the respective wash buffers supplied as part of the WN virus IgM ELISA kit. The enzyme substrate used in all our ELISAs was a solution of 3,3′,5,5′ tetramethylbenzidiene (TMB) and H_2O_2 in a citric acid citrate buffer (pH 3.3−3.8) provided again with the InBios kit. Moreover, all the microchip- and microwell-based assays in this work were performed by measuring the absorbance at 650 nm in a commercial microplate reader system (TECAN Infinite M200) operated in the absorbance mode at 37°C. The level of WN viral IgM antibody was estimated in both situations using the kinetic format of ELISA, which our experiments have shown to be a more reliable quantitation approach especially for the microfluidic assays.[34−36] The blank measurements for the reported immunoassays were performed in our study by following a procedure identical to that described above except for replacing the WNRA solution with a normal cell antigen mixture (provided as part of the InBios ELISA kit) in the respective incubation step. The temporal variation in the absorbance signal recorded in these blank experiments was chosen as a measure for the amount of nonspecific binding in the corresponding assay.

RESULTS AND DISCUSSION

Characterization of the Microchip Performance. The PVC holder and microchips employed in our current work were designed to allow absorbance readings on up to 36 fluidic channels as may be seen from Figure 1. These channels were positioned such that the absorbance readings from them corresponded to those recorded by a commercial microplate reader system (TECAN Infinite M200, in our case) for microwells labeled 1, 3, 5, 8, 10, and 12 in rows A, B, C, F, G, and H. The initial assessment of our microchip devices was performed by measuring the absorbance of a bromothymol blue (Sigma-Aldrich) solution prepared in a 10 mM sodium tetraborate buffer (pH 9.2) introduced into its microchannels. It was determined that this indicator species exhibited the maximum value in its absorption spectrum around 600 nm for the chosen buffer solution. In Figure 3a, we have included a set of absorbance measurements at this wavelength made on solutions containing different concentrations of bromothymol blue (BTB) placed within standard microchannels (with no mirrors) and microwells. As may be seen from the figure, a linear trend was observed between the two quantities with a relatively small y-intercept value for the best-fitted lines to these measurements, which corresponded to the absorbance reading for the blank sample. Interestingly, the blank absorbance recorded for a 10 mM sodium tetraborate solution was only 0.004 units higher for the glass microchips compared with that recorded for the microwells (0.041 versus 0.037). This observation suggests that the amount of light being reflected/scattered by the glass microchips and the polystyrene microwell plates were likely quite similar to that in our microplate reader instrument. However, the standard deviation for the microchip-based measurements (<10%) was determined to be somewhat larger than that recorded for the microwells (<1%). Observations indicate that the larger variation in the former case mostly occurred due to the absorbance readings being more sensitive to the positioning of the microchip within the holder than that of the microwell plate. Figure 3a also shows a proportional increase in the slope of the best-fitted lines to the microchip-based measurements, that is, sensitivity of the microchip-based absorbance detection method, with the depth of the channel employed establishing

https://dx.doi.org/10.1021/acs.analchem.0c01961
Anal. Chem. 2020, 92, 13050−13057

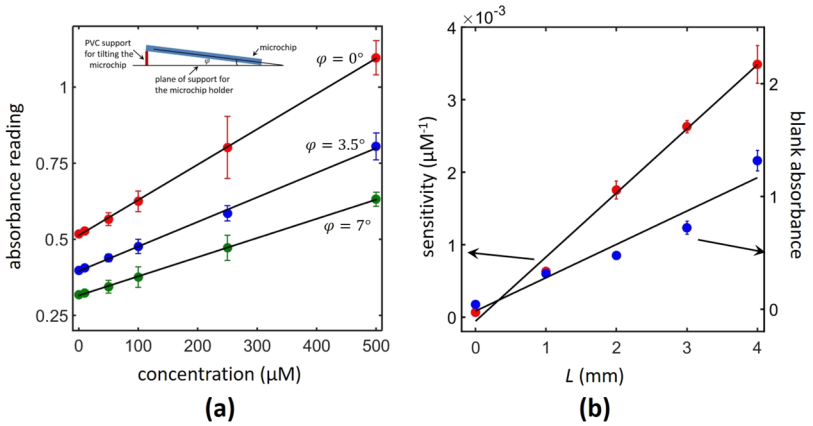

Figure 4. (a) Effect of tilting the microchip device above the horizontal plane on absorbance measurements made on 5 mm-wide and 30 μm-deep glass channels with L set equal to 1 mm. The equations for the best-fitted lines to the data obtained for 0, 3.5, and 7° tilt angles were $y = 1.16 \times 10^{-3}x + 0.513$, $y = 8.08 \times 10^{-4}x + 0.395$, and $y = 6.3 \times 10^{-4}x + 0.315$, respectively. (b) Observed variations in the blank value and sensitivity of the absorbance measurements with the extent of axial overlap of the mirror surfaces along the top and bottom glass plates (L). The measurements included in this subfigure were obtained with 5 mm-wide and 30 μm-deep microchannels when $\varphi = 7°$. All error bars included in this figure were estimated based on five independent experiments performed in different microchannels using aliquots of the same sample.

the validity of Beer−Lambert's law for our data set. Furthermore, the corresponding slope for the measurements made on microwells was determined to be about 62 times larger than that for the 30 μm-deep channel, which again compares well with the ratio of the optical path lengths in these systems. This ratio was estimated to be ∼65 for a 75 μL BTB sample introduced into a 7 mm i.d. microwell as was the case in our measurements.

Having determined the sensitivity of our absorbance detection in standard microwells and glass microchannels, we proceeded with similar measurements made on microchips with aluminum layers deposited on their top and bottom glass plates. A set of such measurements has been included in Figure 3b in which the centers of the microchannels were aligned with these of the microwells and the effects of the extent of axial overlap of the mirror surfaces along the top and bottom plates were assessed on the absorbance readings. This extent of overlap denoted by the parameter L in Figure 1a determined the number of the possible reflections of the incident beam in the microchannel and was predicted to offer larger optical path lengths in our system with an increase in its magnitude. The noted trend was indeed observed in our measurements as evident from the slopes of the best-fitted lines to the microchip-based measurements shown in Figure 3b. For example, the line corresponding to the L = 1.5 mm case in this figure was determined to be about 25 times steeper than that recorded for a 30 μm-deep channel with no mirror surfaces. Moreover, this improvement in the detection sensitivity was observed to scale linearly with L as predicted by Beer−Lambert's law. Unfortunately, however, it was noticed that the absorbance reading for our blank sample also increased considerably for larger values of L. This observation nevertheless is consistent with the idea that a longer aluminum mirror along the top glass plate prevents a greater amount of the incident light from reaching the detector. Consequently, the blank reading in our experiments, that is, the y-intercept value for the best-fitted line to the absorbance measurements, was seen to increase with the larger axial overlap of the mirror surfaces, reducing the amount of light transmitted to the detector from 91 to 6.8% on increasing L from 0 to 1.5 mm in the 30 μm-deep channels. For this choice of the channel depth, the absorbance reading recorded by the microplate reader was in fact noticed to saturate at a value of 3 for various concentrations of the BTB indicator when L was set to 2 mm. It must be mentioned that the TECAN Infinite M200 system employed in this work reports the spot size of the absorbance light beam to be 0.7 mm in diameter, which is also more or less consistent with the trend in the microchip-based blank measurements reported above.

In an attempt to reduce the amount of light blocked by the aluminum mirror deposited on the top glass plate, we also investigated the effect of tilting our microchips on the absorbance readings. To this end, the angle of tilt denoted by the symbol φ in Figure 4a was adjusted in our setup by attaching a machined piece of the PVC block with a 3 × 3 mm cross-section but with varying heights (2.9 and 5.8 mm) to the microchip device using a UV curable glue (Norland Products Inc.). Two nonzero values of φ, that is, 3.5 and 7°, were realized employing this design, yielding the data set shown in Figure 4a for a microchip device with 30 μm-deep channels and L set equal to 1 mm. The figure shows an increase in the amount of transmitted light to the detector from 30.7 to 48.4% for a blank sample upon changing φ from 0° to 7°, which expectedly also came with 85% decrease in the sensitivity of the corresponding absorbance measurements. Notice that this observation is consistent with the fact that an increase in the value of φ automatically leads to a larger angle of incidence for the incoming light beam, that is, θ in Figure 1a, which in turn reduces the number of reflections it can undergo in the microchannel. However, the reduced blank absorbance for the tilted microchips allowed use of longer mirrors and thereby larger values of L in our system. It was subsequently established that mirror designs with L as large as 4 mm could be employed in our microchip devices with 5 mm-wide and 30 μm-deep channels for $\varphi = 7°$. For the noted choice of the channel dimensions and tilt angles, the observed variations in the blank value and sensitivity of our absorbance measurements with L have been shown in Figure 4b. While the figure shows a highly linear increase in the measured sensitivity with the extent of axial overlap of the mirror surfaces along the top and bottom glass plates, this variation for the blank absorbance value was somewhat nonlinear particularly

https://dx.doi.org/10.1021/acs.analchem.0c01961
Anal. Chem. 2020, 92, 13050−13057

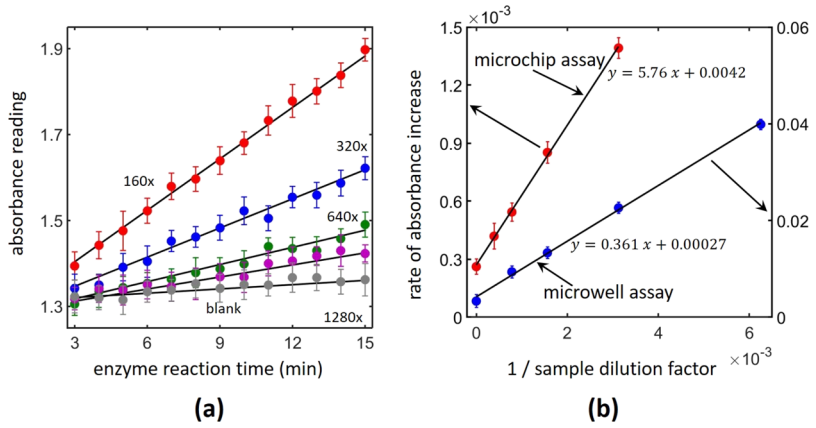

Figure 5. (a) Variation in the absorbance reading as a function of the enzyme reaction time in a 5 mm-wide, 30 μm-deep channel with L = 4 *mm* and φ = 7°. The number associated with the curves refers to the sample dilution factor used in the respective assay. All error bars included in this sub-figure were estimated based on five independent experiments performed in different microchannels using aliquots of the same sample. (b) Variation in the temporal rate of increase in the absorbance reading with the reciprocal of the sample dilution factor used in the microchip- and microwell-based assays. The error bars here correspond to the standard deviation in the slope of the best-fitted line to the absorbance readings when plotted as a function of the enzyme reaction time as in sub-figure (a).

for larger values of L. A maximum improvement in the detection sensitivity by a factor of 52.1 was recorded employing the reported multireflection approach over a standard microchip device with no mirrors upon employing the best allowed design parameters in our setup, that is, L = 4 mm and φ = 7°. However, this result was accomplished at the expense of increasing the blank absorbance value to about 1.32 from 0.041, which compromised the linear/dynamic range of our microchip-based absorbance measurements. Nevertheless, the reported microchip design with 30 μm-deep channels compensates a majority of its inherent deficit in detection sensitivity (about 62-fold) relative to that measured for standard microwells containing 75 μL samples.

Note that it may be possible to further increase the detection sensitivity of our microchips by tilting them beyond φ = 7° potentially allowing the use of more overlapping mirrors, that is, L > 4 mm, in our design. However, for the microchip holder reported here, φ = 7° was the largest tilt angle realizable in our system, which limited the allowed value of L to $\lesssim$4 mm before the mirror surface starts preventing a majority of the incident beam from entering into the microchannel and consequently saturating the blank absorbance reading recorded by the microplate reader. It must be also pointed out that some of the data points used in Figure 3 have been shared with those included in Figure 4 to establish consistency between the various data sets obtained from our experiments. For example, the data set for L = 1 mm in sub-Figure 3b is the same as the one corresponding to the φ = 0° case in sub-Figure 4a. Similarly, the data point representing sensitivity when L = 1 mm in sub-Figure 4b is simply the slope of the best-fitted line to the data set obtained for φ = 7° in sub-Figure 4a.

ELISA Quantitation. Having demonstrated a microchip design with a comparable detection sensitivity to that realized on a microwell plate, we applied this design to demonstrate a microfluidic ELISA method quantitated using the absorbance technique. In the noted assay, the level of WN viral IgM antibody in human serum samples was determined by monitoring the absorbance reading as a function of the enzyme reaction time (kinetic ELISA) over a 15-min period. Figure 5a includes data obtained from these measurements made on a glass microchip device with 5 mm-wide, 30 μm-deep channels, 4 mm overlap between the mirror surfaces along the top and bottom glass plates, and tilted 7° with respect to the horizontal plane. The figure shows a linear increase in the absorbance reading with the enzyme reaction time validating that this reaction was indeed conducted under saturation kinetic conditions as intended. In this situation, the temporal rate of increase in the absorbance reading served as a measure for the analyte concentration that then provided a response curve for our measurements. Because the WN viral IgM antibody sample used in our experiments was the positive control obtained as part of the commercial InBios ELISA kit, we only had a qualitative measure for the analyte concentration in the sample in terms of its dilution factor. For the samples employed in this work, Figure 5b shows the temporal rate of increase in the absorbance signal to vary linearly with the reciprocal of the sample dilution factor, establishing our measurements to be in the linear dynamic range for both the microchip- and microwell-based assays. These response curves were then used to estimate the limits of detection for the corresponding ELISA methods, which were determined to be a sample dilution factor of 1878 and 3338 for the microchip- and microwell-based assays, respectively. The noted detection limits were computed as the dilution factors at which the temporal rate of increase in the absorbance signal equaled to that for the blank sample plus three times its standard deviation based on the equation of the relevant best-fitted line shown in Figure 5b. It must be pointed out that while the detection limits for the microchip- and microwell-based ELISAs were found to be comparable in our experiments, the sensitivity of the former assays exceeded that of the latter by nearly 16-fold. This likely occurred due to the larger surface area-to-volume ratio as well as a lower diffusional resistance in the microchips, which may have resulted in a higher capture efficiency of the analyte molecules on its ELISA surface. For example, although the microchannels and microwells employed in our ELISA experiments had similar surface areas to which the samples were exposed (0.5 mm^2 versus 0.81 mm^2), the sample volumes used within them were significantly different (1.5 μL versus 75 μL). This meant that if the same fraction of analyte molecules were captured on the microchip- and microwell-based assay surfaces maintaining identical activity,

https://dx.doi.org/10.1021/acs.analchem.0c01961
Anal. Chem. 2020, 92, 13050−13057

the rate of increase in the concentration of the enzyme reaction product (TMB diamine) would be the same in the two systems. However, the diffusional time scale for the analyte species to reach the assay surface in the microchannels was estimated to be about 2 s versus 11 hrs in the microwells for an analyte diffusivity of 10^{-6} cm^2/s, assuming a diffusional length scale of 15 μm and 2 mm, respectively, in these systems. In this situation, the higher sensitivity of the microchip-based ELISAs can be well justified, although these assays also showed a substantially higher variation in the measurements, that is, greater noise levels. As a result, this greater sensitivity did not translate to any gains in the limit of detection for the microchip devices, yielding a value for this figure of merit very similar to that measured on microwell plates.

We would like to point out that while the experimental data points shown in Figure 5a appear to be randomly distributed around the best-fitted lines, this observation is valid only upon averaging data sets obtained from multiple experiments. For the individual data sets, however, minor drifts from the best-fitted line with magnitudes comparable to those of the error bars shown in Figure 5a are typically observed in the absorbance readings during the enzyme reaction period. Although the origin for these drifts is unclear at this point, they are likely a result of the nonidealities, for example, thermal effects, mechanical disturbances, etc., in our system. Additionally, we would like to note that while the microfabrication approach outlined here yields reproducible data sets in general, we have typically been unsuccessful in using about 5% of our microchannels due to small parts of the metal layer peeling off from the glass surfaces during the fabrication steps. Such damaged mirror surfaces have been observed to significantly compromise the detection sensitivity of our microchips and have been therefore not used in performing any of the measurements included in this manuscript.

CONCLUSIONS

To summarize, we report absorbance detection in multireflection microfluidic channels using a commercial microplate reader system at similar sensitivities to that realized on standard microwells for a given concentration of the absorbing species in the sample. The noted multireflection functionality was realized by patterning aluminum mirrors on the top and bottom plates of our microchip to guide the probing light beam along the channel axis, thus increasing the optical path length in the process. Our study showed that this improvement in absorbance detection strongly depends on the extent of axial overlap of the mirror surfaces patterned on the top and bottom plates of the microchip as well as the tilt angle for the device relative to the horizontal plane. The mirror surfaces unfortunately also reflected back a fraction of the incident beam, preventing it from reaching the detector and thereby increasing the black absorbance in the system. In any case, an enhancement in the detection sensitivity by as much as 52-fold was realized using our microchip devices, which then were applied to demonstrate a microfluidic ELISA method quantitated using the absorbance technique. While a similar detection limit for the WN viral IgM antibody was observed using our multireflection device and the standard microwell plates, the assay sensitivity was noted to be about 16-fold greater in the former case, likely due to the larger surface area-to-volume ratio and lower diffusional resistance in the microchannels. Unfortunately, our microchip-based ELISAs also yielded a higher noise level in the measurements, which prevented them from translating any of the sensitivity benefits to lower detection limits for the analyte species. Nevertheless, the ability to integrate preconcentration methods in microfluidic systems[35] offers the opportunity to allow further improvements in their limits of detection likely permitting significantly more sensitive measurements on this platform compared with that possible on microwell plates. Interestingly, the multireflection approach reported in this work may also be applied to enhancing the sensitivity of luminescence-based sensing techniques. For example, the optical path length in fluorescence detection systems can be increased using mirror surfaces following an approach similar to that employed in our current absorbance measurements. Moreover, upon carefully designing the shape, size, and curvature of these reflective surfaces, it may be possible to increase the amount of fluorophore emission reaching the detector, thereby further improving analyte detectability. We are currently pursuing these ideas to perform sensitive micro-/nanofluidic assays and expect to publish our findings from such studies in the future.

AUTHOR INFORMATION

Corresponding Author

Debashis Dutta − *Department of Chemistry, University of Wyoming, Laramie, Wyoming 82071, United States;* orcid.org/0000-0003-0938-3151; Email: ddutta@uwyo.edu

Authors

Naoki Yanagisawa − *Department of Chemistry, University of Wyoming, Laramie, Wyoming 82071, United States*

Sakur Mahmud − *Department of Chemistry, University of Wyoming, Laramie, Wyoming 82071, United States*

Complete contact information is available at: https://pubs.acs.org/10.1021/acs.analchem.0c01961

Notes

The authors declare no competing financial interest.

ACKNOWLEDGMENTS

This research work was supported by a grant from the National Institutes of Health (1R15AG045755-01A1). D.D. also acknowledges the funds from the National Science Foundation and Wyoming INBRE program through grants CHE-1808507 and P20GM103432, respectively, that help completing some of the experiments included in this manuscript.

REFERENCES

(1) Dolnik, V.; Liu, S. R.; Jovanovich, S. *Electrophoresis* **2000**, *21*, 41−54.

(2) de Mello, A. *Lab Chip* **2002**, *2*, 48N−54N.

(3) Andersson, H.; van den Berg, A. *Sens Actuators B Chem.* **2003**, *92*, 315−325.

(4) Ng, A. H. C.; Uddayasankar, U.; Wheeler, A. R. *Anal. Bional. Chem.* **2010**, *397*, 991−1007.

(5) Sia, S. K.; Whitesides, G. M. *Electrophoresis* **2003**, *24*, 3563−3576.

(6) Napoli, M.; Eijkel, J. C. T.; Pennathur, S. *Lab Chip* **2010**, *10*, 957−985.

(7) Piruska, A.; Gong, M.; Sweedler, J. V.; Bohn, P. W. *Chem. Soc. Rev.* **2010**, *39*, 1060−1072.

(8) Jokerst, J. C.; Emory, J. M.; Henry, C. S. *Analyst* **2012**, *137*, 24−34.

(9) Yetisen, A. K.; Akram, M. S.; Lowe, C. R. *Lab Chip* **2013**, *13*, 2210−2251.

(10) Verpoorte, E. *Electrophoresis* **2002**, *23*, 677−712.
(11) Dittrich, P. S.; Manz, A. *Nat. Rev. Drug Discov.* **2006**, *5*, 210−218.
(12) Howorka, S.; Siwy, Z. *Chem. Soc. Rev.* **2009**, *38*, 2360−2384.
(13) Kim, S. J.; Song, Y. A.; Han, J. *Chem. Soc. Rev.* **2010**, *39*, 912−922.
(14) Götz, S.; Karst, U. *Anal. Bioanal. Chem.* **2007**, *387*, 183−192.
(15) Chen, X.; Zhang, S.; Zhang, L.; Yao, Z.; Chen, X.; Zheng, Y.; Liu, Y. *Biomed. Microdevices* **2017**, 19.
(16) Pamme, N. *Lab Chip* **2006**, *6*, 24−38.
(17) Ding, X. Y.; Li, P.; Lin, S. C. S.; Stratton, Z. S.; Nama, N.; Guo, F.; Slotcavage, D.; Mao, X. L.; Shi, J. J.; Costanzo, F.; Huang, T. J. *Lab Chip* **2013**, *13*, 3626−3649.
(18) Louer, A. C.; Plecis, A.; Pallandre, A.; Galas, J. C.; Esevez-Torres, A.; Haghiri-Gosnet, A. M. *Anal. Chem.* **2013**, *85*, 7948−7956.
(19) Beyor, N.; Seo, T. S.; Liu, P.; Mathies, R. A. *Biomed. Microdevices* **2008**, *10*, 909−917.
(20) Chen, H.; Fang, Q.; Yin, X. F.; Fang, Z. L. *Lab Chip* **2005**, *5*, 719−725.
(21) Wang, J. *Talanta* **2002**, *56*, 223−231.
(22) Pumera, M. *Talanta* **2007**, *74*, 358−364.
(23) He, X. W.; Chen, Q. S.; Zhang, Y. D.; Lin, J. M. *Trac-Trends Anal. Chem.* **2014**, *53*, 84−97.
(24) Chen, C. H.; Tsao, T. C.; Tang, J. L.; Wu, W. T. *Sensors* **2010**, *10*, 4794−4804.
(25) Lee, S. M.; Jeong, M. Y.; Saini, S. S. *J. Lightwave Technol.* **2012**, *30*, 1025−1031.
(26) Morhart, T. A.; Read, S. T.; Wells, G.; Jacobs, M.; Rosendahl, S. M.; Achenbachc, S.; Burgess, I. J. *Anal. Methods* **2019**, *11*, 5776−5783.
(27) Llobera, A.; Demming, S.; Wilkea, R.; Büttgenbach, S. *Lab Chip* **2007**, *7*, 1560−1566.
(28) Salimi-Moosavi, H.; Jiang, Y. T.; Lester, L.; McKinnon, G.; Harrison, D. J. *Electrophoresis* **2000**, *21*, 1291−1299.
(29) Pena, J.; McAllister, S. J.; Dutta, D. *Biomed. Microdevices* **2014**, *16*, 737−743.
(30) Toh, G. M.; Yanagisawa, N.; Corcoran, R. C.; Dutta, D. *Microfluid. Nanofluid.* **2010**, *9*, 1135−1141.
(31) Bien, D. C. S.; Rainey, P. V.; Mitchell, S. J. N.; Gamble, H. S. *J. Micromech. Microeng.* **2003**, *13*, S34−S40.
(32) Kinde, T. F.; Basile, F.; Dutta, D. *Anal. Chem.* **2013**, *85*, 7167−7172.
(33) Wang, H. Y.; Foote, R. S.; Jacobson, S. C.; Schneibel, J. H.; Ramsey, J. M. *Sens. Actuators, B* **1997**, *45*, 199−207.
(34) Yanagisawa, N.; Dutta, D. *Biosensors* **2011**, *1*, 58−69.
(35) Yanagisawa, N.; Dutta, D. *Anal. Chem.* **2012**, *84*, 7029−7036.
(36) Tsang, V. C. W.; Wilson, B. C.; Maddison, S. E. *Clin. Chem.* **1980**, *26*, 1255−1260.

https://dx.doi.org/10.1021/acs.analchem.0c01961
Anal. Chem. 2020, 92, 13050−13057